ORIGINAL RESEARCH

Failure Rate of Empty and Fluid-Filled Concrete Pipes under High Strain Rates

Asadollah Ranjbar Karkanaki[1]*, Mohsen Parviz[2], Alireza Darvishpour[3] , Mahyar Taheri[4]

Abstract

Considering the importance of the performance of buried concrete pipes under external loads and the role played by concrete specifications and pipe thickness in this regard, the current study analyzed the failure rate and response of concrete pipes buried in three types of soil to a TNT blast load using the Lagrangian-Eulerian method in the nonlinear dynamics software LS-DYNA. The results show that the presence of fluid in the pipe generates an internal pressure, which reduces the deformation of the pipe under the blast load. It was also found that the higher the P-crush of the concrete pipe, the smaller the strain and displacement generated under the blast pressure. In thicker pipes, sometimes the damage is limited to the outer sections of the shell, and the pipe remains usable. However, in thinner pipes, damage often affects both inner and outer surfaces of the shell, rendering the pipe unusable. The plastic strain generated in Specimen 1 in Soil Type 1 is 85% higher than the acceptable plastic strain of the concrete pipe. Moreover, this value is 87% for Soil Type 2 and 85% for Soil Type 3.

Keywords: Model failure; Concrete pipes; Strain rate; Lagrangian-Eulerian Method; LS-DYNA.

1- Introduction

The impact of blasts on buried pipelines is a function of the burial depth, the dimensions of the pipe, the applied load, the blast distance, the material of the pipe, the soil material, and the internal pressure of the pipe. In 2007, Kouretzis et al. introduced an analytical method for determining the pressure applied to buried pipes by blast loads. They modelled the pipe as a 3D thin cylindrical shell without structure-soil interactions, while they modelled the waves with radial attenuation. Finally, the results were compared with the results of numerical modelling, and it was demonstrated that the proposed method was more accurate than numerical models [1]. In another study, Francini et al. (2008) investigated the effects of construction and blast vibrations on buried pipes. In this work, four types of concrete pipes were installed in a coal field, and the pressure applied by the blast force was measured

✉ Corresponding author: Ranjbar.iau@gmail.com

[1] Department of Civil Engineering, East Tehran Branch, Islamic Azad University, Tehran, Iran.
[2] Structural Engineering, Iranian Academic Center for Education, Culture and Research (ACECR), Bushehr Branch, Iran.
[3] Department of Civil Engineering, Robatkarim Branch, Islamic Azad University, Robatkarim, Iran.
[4] Ph.D. student, School of Civil and Environmental Engineering, Oklahoma State Univ, Stillwater, Ok, 74078, USA.

using pressure gauges embedded in the holes [2]. A range of prediction methods is presented to assist damage analysis and design of building components against explosion effects by Riedel et al. (2010) [3]. In 2011, Noorzad et al. studied the extent of damage done to continuous buried pipes along the blast load. In this study, the effects of burial depth, blast distance, pipe material, and soil type were investigated, and it was found that the pipe's dimensions and thickness affected its resistance to the blast, and that the pipes made of materials with a higher modulus of elasticity exhibited better elastic behaviour under the blast force [4]. In a study by Yan (2012), the dynamic response of the pipes buried in soft soils was analysed by the nonlinear dynamics and Lagrangian-Eulerian method in the LS-DYNA software. In this study, the effects of burial depth and distance from the blast site were investigated, and it was shown that the upper half of the pipe experienced compression, while its lower half underwent tension [5]. In 2013, Xu et al. simulated the deformation of buried pipes under a blast force for a variety of pipe dimensions and blast distances. This simulation showed that the damage done to the pipe was closely related to the pipe's diameter and its distance from the blast site [6]. In 2013, Jing et al. used the Arbitrary Lagrangian-Eulerian method in LS-DYNA to assess the effects of three types of blasts on buried pipes. They reported that 3 and 5 blasts did not seriously damage the pipe, but 10 blasts created a pressure higher than the pipe's strength, which caused serious damage [7]. In 2013, Orton et al. analysed the strength of CFRP-wrapped concrete components under a blasting force, and proposed a method for predicting the response of concrete slabs to cracking, direct shear, waves, and shell behaviour, as well as several equations for estimating the capacity of each behaviour. The results of this study showed that the proposed method could easily predict the maximum deformation of concrete slabs [8]. In a parametric study by Mokhtari (2015) on the mechanical performance of steel pipes under sub-surface blasts when considering internal pressure, pipe dimensions, and blast distance, it was reported that pipe deformation and maximum equivalent strain were more influenced by the internal pressure than by the diameter-to-thickness ratio [9]. In 2015, Almatian et al. analysed the effects of blasts on the stress and strain variations of buried water pipes using Abaqus and Autodyne software applications, and they reported that the steel pipe could not withstand the blast force of 10 kilograms of TNT exploded on the surface [10]. In 2016, Abedi et al. proposed an analytical method for estimating the dynamic response of buried pipes to blast waves of different magnitudes. Using this method, they concluded that in intact limestones, blasts stronger than a 40-kg TNT load were not permissible [11]. In 2016, Mokhtari studied the response of buried CFRP-reinforced steel pipes to subsurface blasts as well as the effects of burial depth, blast distance, and blast magnitude in this regard [12]. This study showed that the pipes with higher internal pressure were more resistant to the blasts. However, in the event of a rupture in the CFRP wrapping, the pressure would become concentrated on the ruptured region. Zhang et al.

investigated the effects of pipe thickness, internal pressure, and burial depth, as well as the TNT load on the dynamic response of the pipe to blasts. This investigation showed that the higher the TNT load and the lower the burial depth, the greater the pressure along the perimeter axis and the deformation of the pipe [13]. In 2017, Parviz et al. studied the dynamic response of water inside buried steel and concrete pipes to blast force while taking into account the effects of different parameters related to water, TNT, pipe, soil, and air [14]. This study indicated that the blast force did less damage to the pipes buried in lower density soils as such soils act as a damper. In 2017, Vivek et al. conducted a series of laboratory simulations by using a shock tube to generate wave bursts in order to analyse the effects of spherical blasts on pipelines [15]. This study reported that the pressure damping increased with depth and that the pipe deformed after receiving the shock wave of the explosion. In 2017, Adibi et al. conducted a parametric study on the effects of blast load, pipe thickness, burial depth, and concrete cover on high-pressure gas pipes, and they reported that as burial depth increased, pipe deformation under the blast force decreased by up to 71% [16]. Although the importance of the damage that can be done to concrete pipes by blast waves and the effects of parameters such as P crush on the pipe deformation and strains are widely accepted, there has been no comprehensive study on the effects of a fluid on the pipe deformation and how strains effect the pipe fracture. In 2018, Guo Y et al, a numerical simulation method of buried parallel natural gas pipelines leakage-induced explosion based on TNT equivalent was presented. Then, the deformation and fracture failure of natural gas pipeline caused by shock waves under different spacing between two buried parallel pipelines were analyzed and discussed [17]. In 2021, Kakaei R *et al*, the effect of using the GFRP blanket on the performance of pressurized API 5 L-X65 buried pipelines that are prone to an explosion have been studied using the finite element method [18].

This study investigates factors affecting the resistance of an empty concrete pipe and a concrete pipe filled with fluid to the blast load and the pressure applied from the soil using the ALE solution method, which allows the interaction between the soil and the structure to be investigated.

2- Constitutive Model

2-1- Explosive Model

The explosive charge was simulated using the Jones-Wilkins-Lee (JWL) equation of state and the corresponding constitutive model in the LS-DYNA software, called MAT_HIGH_EXPLOSIVE_BURN. The characteristics of the explosive model were set according to those used by Yan et al. The pressure equation in the software was defined as follows [14]:

$$P = A\left[1-\frac{\omega}{V R_1}\right]e^{-R V_1} + B\left[1-\frac{\omega}{V R_2}\right]e^{-R_2 V} + \frac{\omega E}{V} \quad (1)$$

Where P is the pressure and A, B, R_1, R_2, and ω are the coefficients that depend on the type of explosive. Moreover, V is the volume of the explosive, and E is the characteristic explosion energy. Table 1.

Table 1. TNT Charge Parameters

Material Properties	Density (kg/m3)	B (Gpa)	A (Gpa)	P_{CJ}(Gpa)	V_D(m/s)
Numerical Values	1630	6930	21	374	3.23
Material Properties	R_1	R_2	ω	E_0(J/kg)	V
Numerical Values	4.15	0.95	0.38	1	6.0e+09

2-2- Air Model

The air was modelled using NULL MATERIAL and the linear Equation of State (EOS) [5]. In the LS-DYNA software, the pressure equation for the constitutive model of the air was defined as follows:

$$P = C_0 + C_1\mu + C_2\mu^2 + C_3\mu^3 + \left(C_4 + C_5\mu + C_6\mu^2\right)E_0 \quad (2)$$

Where the parameter P is the pressure, μ is a function of ρ, and ρ_0 is the reference density. Moreover, c_0 to c_5 are the equations of constant coefficients. The parameter E0 is the initial internal energy of the reference specific volume per unit Table 2. [14]

Table 2. Air Parameters

Material Properties	Density (kg/m3)	C_3	C_2	C_1	C_0
Numerical Values	1.29	6930	21	374	3.23
Material Properties	C_5	C_4	ρ_0(kg/m3)	E_0(J/kg)	
Numerical Values	0.4	0.4	2.5E+5	1	

2-3- Concrete Pipe Model

The constitutive model of the concrete pipes was created using the Johnson–Holmquist model. This model can be used for concrete that is under high compression. Equivalent resistance is expressed as a function of pressure, tension and damage. Pressure is expressed as a function of volumetric pressure and includes the effect of permanent crushing.

This damage accumulates as a function of plastic volume strain, equivalent plastic strain, and pressure [19] Many concrete material models have been extensively studied by observing impact simulation to observe the fracture response of cementitious material models. Reinforced concrete should be studied more extensively because it is sometimes difficult to quantify the rebar embedded in a simulation [20] In the model, the above material is defined as the following equation to determine the strength and normal equivalent stress.

$$\sigma* = \frac{\sigma}{f_{\ni c}} \quad (3)$$

Where σ is the real equivalent stress, and f_c is the quasi-static uniaxial compressive strength. This expression is defined as dependent on pressure and strain velocity.

$$\sigma = (A(1-D) + BP^{*N})(1 + C * ln\left(\frac{\varepsilon^*}{\varepsilon_0}\right)) \quad (4)$$

Equation (4) states that as a material experiences higher confining pressures and increasing strain rates, the material's yield strength will also increase. The material constants A (cohesive strength coefficient), B (pressure coefficient), C (strain rate coefficient), and N are determined by fitting the model to experimental data. The parameter D is a scalar damage variable, described in greater detail in the following section, where damage can span a value from 0 to 1 and relates to the damage state of a material. When D = 0, the material is undamaged and its strength corresponds to the strength of the material fully intact. While D = 1, the material is damaged and its strength corresponds to the strength of the material at a fully fractured state which only retains the least confined shear strength. The normalized pressure is given as the pressure divided by the unconfined compressive strength.

Damage variables accumulate and can be defined by the accumulation of volumetric plastic strain ($\Delta \mu_{pl}$) and equivalent plastic strain which ($\Delta \varepsilon_{pl}$) which are caused by the volumetric compaction and deformation/fracture respectively. Damage is calculated by dividing the summation of plastic volumetric strain and equivalent plastic strain by the plastic strain to fracture at constant pressure (ε_f). The equation for damage accumulation and plastic strain to fracture are given by the Eqn. (5) and (4) respectively.

$$D = \sum \frac{\Delta\varepsilon_{pl} + \Delta\mu_{pl}}{\varepsilon_f} \quad (5)$$

$$\varepsilon_f = D1(P^* + T^*)^{D2} \quad (6)$$

A material's hydrostatic pressure response to volumetric strain is described by Holmquist as having three distinct regions in compression. The first region is a linear section governed by the materials elastic properties from zero to predetermined crush values for pressure and volumetric strain acquired from experimental data. Any deformation acquired in this region is recoverable since it's all elastic. The second region starts from the crush values of pressure and volumetric strain ($\mu crush$, $Pcrush$) which occurs from the onset of concrete crush to its locking region. This section is the transition region that relates to concrete plasticity and produces a modified unloading path that is interpolated from adjacent regions. The third region starts from the corresponding

point ($\mu lock, Plock$) and is associated with a material that is fully dense (air voids in material are completely compressed). The three distinct regions showing the hydrostatic pressure and volumetric relationship for HJC is shown schematically in Figure 1. [20]

Volumetric strain is also defined as a function of current density (ρ) and reference density (ρ_o). The volumetric strain equation has been given in Equation (7). For the concrete material model, we consider the important specifications of Table 1.

$$\mu = \frac{\rho}{\rho_0} - 1 \quad (7)$$

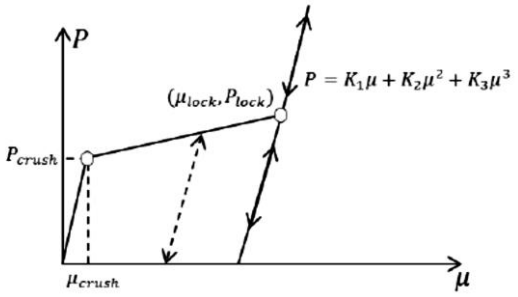

Figure 1. HJC hydrostatic pressure and volumetric strain relationship [20]

$$P = K_e\mu \quad (8)$$

$$P = K_1\mu + K_2\mu^2 + K_3\mu^3 \quad (9)$$

The various variations of K in the previous equation are all material constants related to the volumetric modulus (K_e).

Two pipe dimensions were defined, i.e., one with an inner diameter of 0.2m and an outer diameter of 0.4m, and another with an inner diameter of 0.3m and an outer diameter of 0.4m. In addition, two types of concrete materials were defined, i.e., Type I with a density of 2440 kg/m3, a strength of 48 MPa, a final strain (before fracture) of 0.01, and PC of 1.6 Mpa, Table 3. [21]. and Type II with a density of 2500 kg/m^3, a strength of 43.6 MPa, a final strain (before fracture) of 0.01, and PC of 14.53 Mpa, Table 4. [22].

Table 3. Parameters of Concrete Type I

Material Properties	Density (kg/m3)	G (Pa)	A	B	C	N	Fs (Pa)
Numerical Values	2440	14.9e9	0.79	1.60	0.007	0.61	48.0e6
Material Properties	T (Pa)	EPSO	EFmin	SF_{MAX}	U_C	P_1 (Pa)	U_L
Numerical Values	4.0e6	0.001	0.01	7.0	0.001	0.8e9	0.1
Material Pro…	D_1	D_2	K_1(Pa)	K_2(Pa)	K_3(Pa)	Fs	P_C (Pa)
Numerical Values	0.04	1.0	85e9	17.1e9	20.8e9	0.3	1.6e6

Table 4. Parameters of Concrete Type II

Material Properties	Density (kg/m^3)	G (Pa)	A	B	C	N	Fs (Pa)
Numerical Values	2500	12.5e9	0.79	1.60	0.007	0.61	43.6e6
Material Properties	T (Pa)	EPSO	EFmin	SF_{MAX}	Uc	P_1 (Pa)	U_L
Numerical Values	4.09e6	0.001	0.01	7.0	0.00087	1.0e9	0.072
Material Properties	D_1	D_2	K_1(Pa)	K_2(Pa)	K_3(Pa)	Fs	P_C (Pa)
Numerical Values	0.0038	1.0	85e9	17.1e9	20.8e9	0.004	14.53e6

2-4- Soil Model

The soil was modelled using a simple and very practical constitutive model known as SOIL_AND_FOAM,which was developed in 1972 by Krieg et al [23]. This constitutive model was chosen because of its ability to emulate soil behaviour under explosions. Experiments in this study were carried out based on three different soil types, as defined in Table 5. [24].

Table 5. Parameters of the Soils

Material Properties	Numerical Values of soil 1	Numerical Values of soil 2	Numerical Values of soil 3
Density (kg/m3)	1453	1800	2094
Elastic modulus (MPa)	5.47	47.36	65.3
Shear modulus(MPa)	1.8	16	23
Bulk modulus(MPa)	69	394.7	134
A_0	0	3.3E10	4.361E04
A_1	0	0	2.555 E04
A_2	0.3	0	0.543
Poisson’s ratio	0.48	0.48	0.42
Vs	35.58	94.28	104

2-5- Water Model

Water was modelled with NULL MATERIAL using the Mie–Gruneisen equation of state [5].

$$P = \frac{\rho_0 C^2 \mu \left(1 + \left(1 - \frac{\gamma_0}{2}\right)\mu - \alpha \frac{\mu^2}{2}\right)}{\left(1 - (S_1 - 1)\mu - S_2 \frac{\mu^2}{(1+\mu)} - S_3 \frac{\mu^3}{((1+\mu^2))^2}\right)} + (\gamma_0 + \alpha\mu)E \quad (10)$$

In the above equation, P is the pressure (MPa), μ is a function of ρ and ρ_n , while S_1 to S_3, γ_o , and α depend on the constant coefficients. Moreover, E is the internal energy, and C is the velocity of wave propagation in the water. The details of the constitutive model of water are presented in the following table 6.

Table 6. Water Parameters

Material Properties	Numerical Values
Density (kg/m3)	1025
C (m/s)	1.48E+03
S_1	142
S_2	0.33
S_3	0.7
γ_0	0.5

2-6- Steel Pipe

The constitutive model of the steel pipe was constructed using the PLASTIC KINEMATIC model, in which the material exhibits a bilinear behaviour Table 7 [7].

Table 7. Parameters of the Steel Pipe

Material Properties	Density (kg/m3)	Elastic modulus (GPa)	Poisson's ratio	Yield stress (MPa)	Tangent modulus (GPa)
Steel pipe	7850	210	0.3	360	13.5

3- Geometry Modeling

The authors developed five constitutive models for the soil, the TNT, the air, the fluid, the steel pipe, and the concrete pipe. The pipe was modelled below the TNT at a depth of 1.45m from the ground surface. The TNT was modelled as a charge buried under the ground surface. Considering the symmetry of the defined geometry, only one-fourth of the geometry with the dimensions of 2×1.8×0.6 was modelled to accelerate the computations.

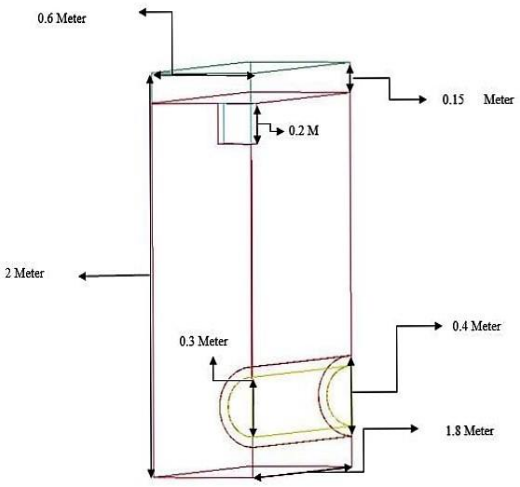

Fig. 1. Schematic Diagram of the System with Relevant Dimensions.

According to the Fig.2, the models were constructed using the 8-node Solid-164 elements. In the nonlinear structural analysis, the Eulerian-Lagrangian method was used to prevent element rupture due to large deformations. For TNT, air, fluid, and soil, the constitutive models were constructed using the Eulerian-Lagrangian meshes. For the pipe, however, the constitutive model was developed using Lagrangian meshes. The pipe-soil-fluid coupling effect was applied using the CONSTRAINED-LAGRANGE-IN-SOLID option. All meshes had a size of 5 cm. Non-reflecting boundaries were used in the outer and bottom surfaces of the model to prevent the echoing of the blast wave.

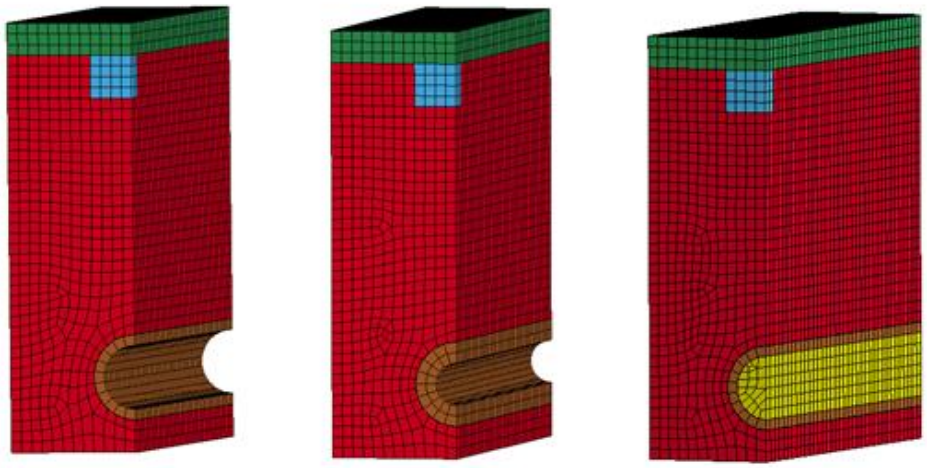

(a) Empty Pipe with a Thickness of 5cm **(b)** Empty Pipe with a Thickness of 10 cm **(c)** Fluid-Filled Pipe with a Thickness of 5cm

Fig. 3. Finite Element Model of the Pipes

The characteristics of the models used in this study are summarized in the table below. It should be noted that each model specimen was simulated with three soil types described in Section 2.4.

Table 8. Description of Model Specimens

Description	Case Name
Type I concrete pipe with a thickness of 5 cm without fluid(empty)	Specimen 1
Type II concrete pipe with a thickness of 5 cm without fluid (empty)	Specimen 2
Type I concrete pipe with a thickness of 10 cm without fluid (empty)	Specimen 3
Type II concrete pipe with a thickness of 10 cm without fluid (empty)	Specimen 4
Type I concrete pipe with a thickness of 5 cm with fluid (fluid-filled)	Specimen 5
Type II concrete pipe with a thickness of 5 cm with fluid (fluid-filled)	Specimen 6

3-1- Validation

To validate the developed model, its results were compared with the results of the numerical model developed by Parviz et al. [14], as can be seen in Fig. 4. This comparison was made between the pressure-time plots obtained from these models and the Yan model. In the current study, the peak blast pressure (580.9 MPa) occurred at t=3.9 ms and the curve showed a decline after t=4 ms. The cause for this decline can be attributed to the effects of the fluid during the explosion since it moves in the opposite direction of the blast wave propagation, thus stabilizing the pipe and damping the blast pressure. It should be noted that the non-reflecting boundary conditions defined for the surface also play an important role in the damping of the pressure with the passage of time.

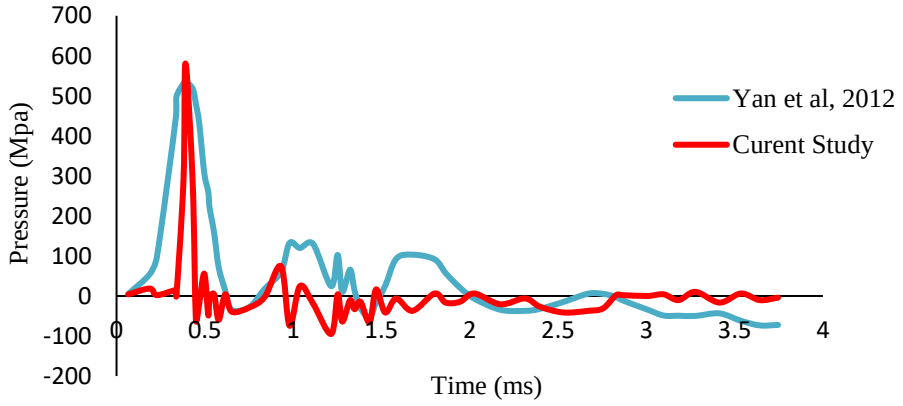

Fig. 4. Pressure-Time Curves Obtained for the Steel Pipe in Soil (for 9 Milliseconds)

4- Results and Interpretation

4-1- Effects of P Crush on Strain and Effects of Strain on Failure in Concrete Pipes

Since the defined concrete types have approximately the same elastic modulus, the effects of P-crush on the strain and deformation in concrete pipes need to be investigated. Fig.5 shows the effects of P-crush on strain in Type I and Type II concrete pipes with different thicknesses.

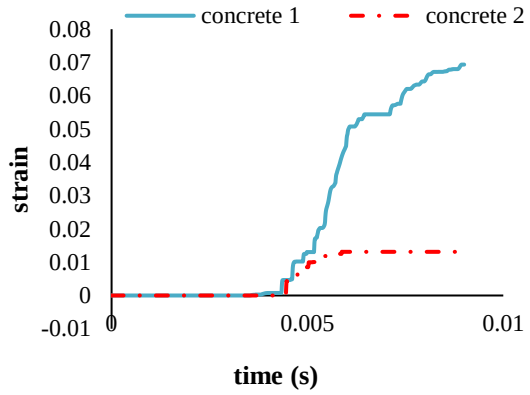

(a) Specimens 1 and 2 in soil type 1

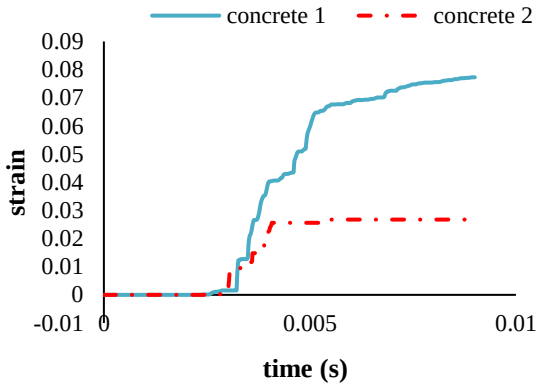

(b) Specimens 1 and 2 in soil type 2

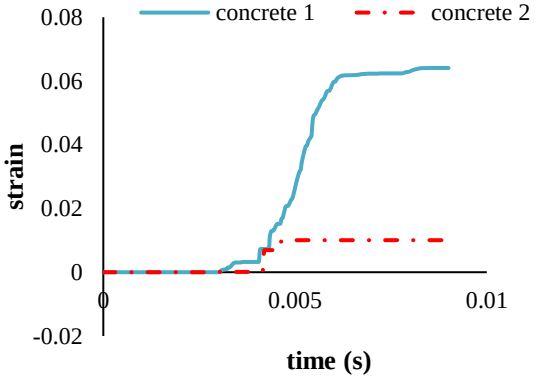

(c) Specimens 1 and 2 in soil type 3

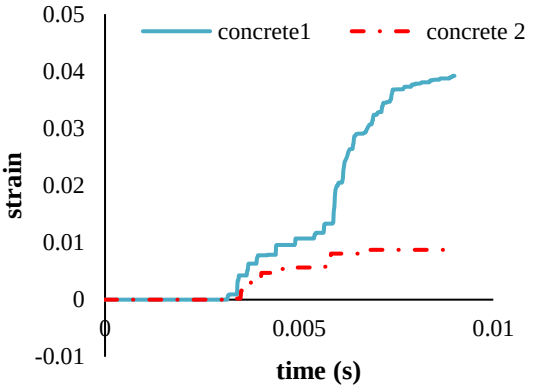

(d) Specimens 3 and 4 in soil type 1

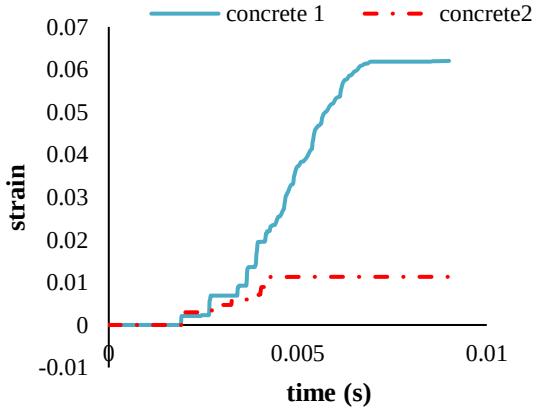

(e) Specimens 3 and 4 in soil type 2

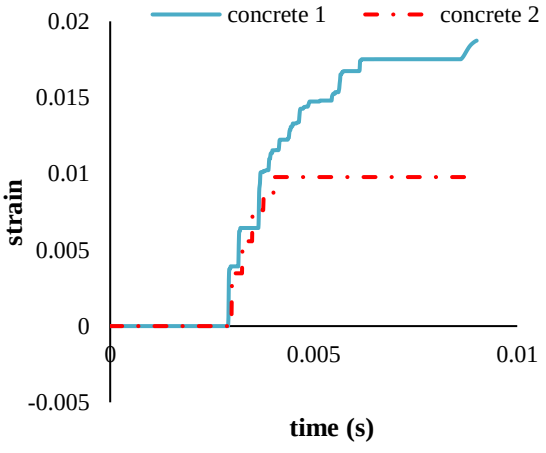

(f) Specimens 3 and 4 in soil type 3

Fig. 5. Comparison of the Strain Created in Specimens 1-4 in Soil Types 1-3

As indicated in Fig.5, strains of Specimens 1 and 2 were compared, while the strains of Specimens 3 and 4 were compared in different soils. According to the results depicted in Fig.5, because of higher p-crush of the Type II concrete compared to Type I, it has shown better behaviour under the blast load. In Soil Type 1, the plastic strain of Specimen 2 is 80% lower than that of Specimen 1. This difference is 66% in Soil Type 2 and 85% in Soil Type 3. A similar difference can also be seen for Specimens 3 and 4. The difference between the strains of Specimens 3 and 4 is 76% in Soil Type 1, 90% in Soil Type 2, and 55% in Soil Type 3.

4-2- Effect of Strain on Damage

Since parameter EF_{min} , which indicates the amount of strain in concrete pipes before failure, can be obtained from the concrete profile, the damage in the pipes with different thicknesses can be analysed based on the results presented in Fig.5.

According to the plastic strain results provided in Fig.5, the plastic strain generated in Specimens 1 and 2 in all three Soil Types causes failure at one or several points, except for Specimen 2 in Soil Type 3, which makes it practically impossible to use a concrete pipe with such profile in such soils. The plastic strain generated in Specimen 1 in Soil Type 1 is 85% higher than the acceptable plastic strain of the concrete pipe. This value is 87% for Soil Type 2 and 85% for Soil Type 3. For Specimen 2, the difference between the plastic strain generated in Soil Type 1 and the acceptable plastic strain is 23%. In Soil Type 2, this difference is 61%, which signifies the occurrence of pipe failure. However, in Soil Type 3, the generated plastic strain is 10% lower than the acceptable threshold, indicating that Specimen 2 will remain operational in this type of soil.

The results obtained for Specimens 3 and 4 in the three defined soil types show that in the pipes where the plastic strain is more than the acceptable threshold, failures with a depth of 2 to 7 centimetres have occurred at the pipe's surface exactly below the blast. However, because of the thickness of the pipes, in none of the cases, the damage level was significant enough to make the pipe unusable. The plastic strain generated in Specimen 3 in Soil Type 1 is 74% higher than the acceptable threshold value for concrete pipes. This difference is 84% in Soil Type 2 and 44% in Soil Type 3. For Specimen 4, the generated strain is 10% below the acceptable threshold value in Soil Type 1, and 20% below acceptable threshold value in Soil Type 3. This indicates that Specimen 4 will remain healthy in these types of soil. However, in Soil Type 2, the plastic strain of this Specimen is 10% higher than the acceptable threshold value, which signifies the strong possibility of failure in some parts of the outer surface of this pipe. Figs. 6 and 7 show the effects of thickness on the damage done to the inner and outer surfaces of the concrete pipes.

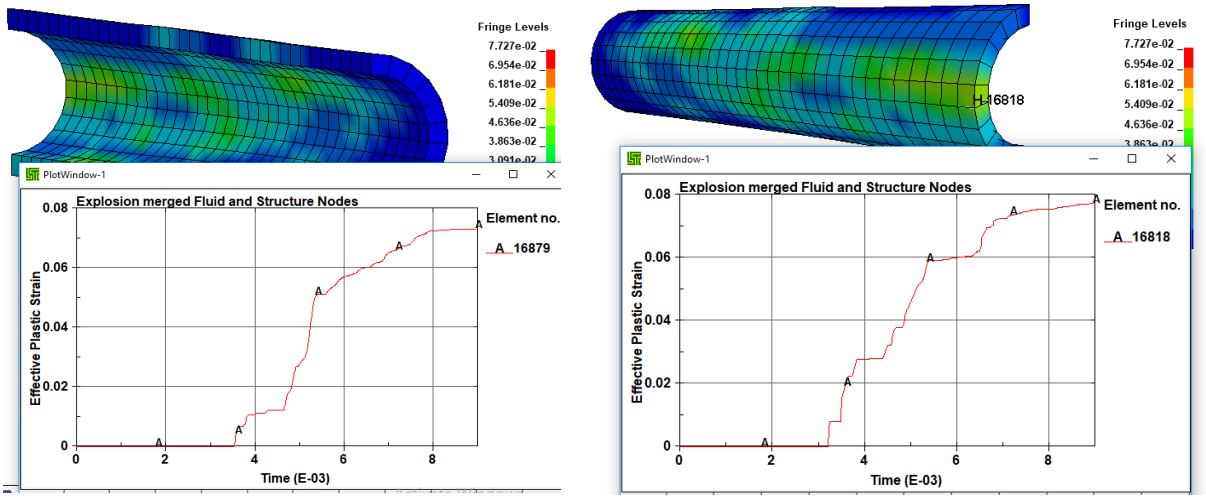

(a) The inner surface of specimen 1 **(b)** The outer surface of specimen 1

Fig. 6. Plastic Strain Created at the Inner and Outer Surfaces of Specimen 1 in Soil Type 2.

As shown in Fig. 6a, the maximum plastic strain created on the inner and outer surfaces of Specimen 1 has exceeded the 0.01 limit, resulting in failure, and since this failure is greater than the acceptable threshold value in both inner and outer surfaces, Specimen 1 is practically useless in Soil Type 2.

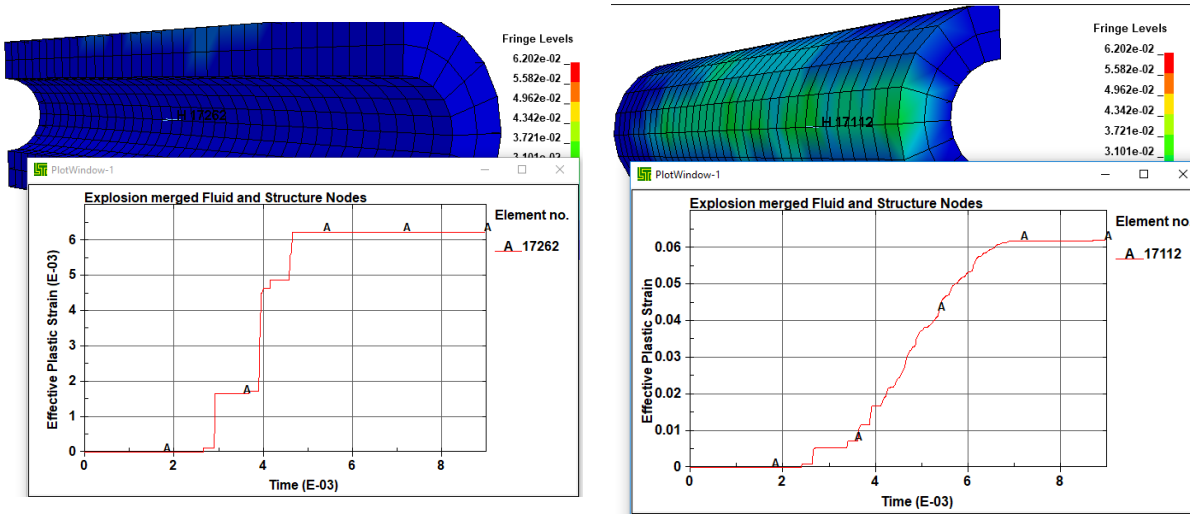

(a) The inner surface of specimen 3 **(b)** The outer surface of specimen 3

Fig. 7. Plastic Strain Created at the Inner and Outer Surfaces of Specimen 3 in Soil Type 2

As can be seen in Fig. 7a, the maximum plastic strain created on the outer surface of Specimen 3 is 83% higher than the permissible plastic strain before failure, which indicates that the failure will occur on the surface of the concrete pipe. However, according to Fig. 7b, since the maximum strain created at the inner surface of the pipe is 0.006 (below the permissible plastic strain limit), the inner

surface of the pipe can be expected to remain completely intact. The depth of the damage to the outer surface of the Type I concrete pipe with a thickness of 10 cm ranges from 4 to 7 cm, indicating that despite the damage, the pipe is still usable. As shown in Fig. 8, strains of Specimens 1 and 3 were compared in 3 different soils.

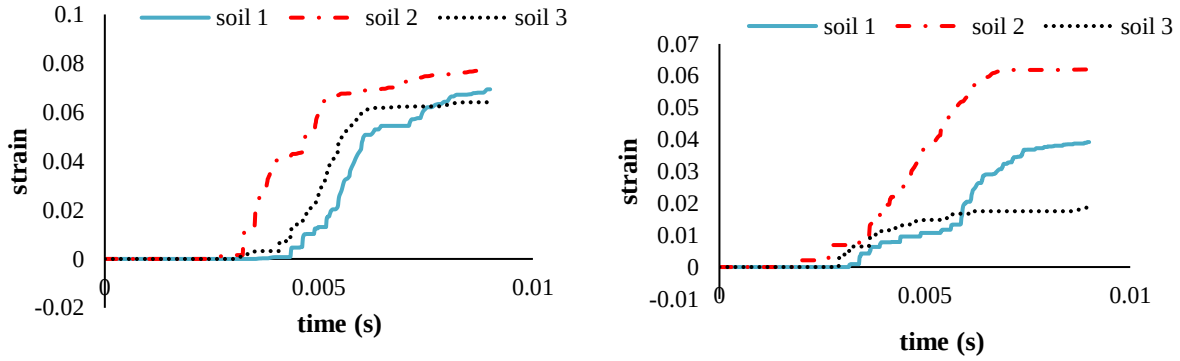

(a) strains in specimen 1

(b) strains in specimen ۳

Fig. 8. Comparison of Plastic Strain Generated in Specimens 1 and 3 in Different Soil Types

4-3- Effects of P-Crush on Deformation of Concrete Pipes of Different Thicknesses, Effects of P-Crush on Deformation

The deformation behaviours of Specimens 3 and 4 under the blast load are very well reflected in the results of the study. Since Type II concrete has 89% lower P-crush than Type I concrete, the deformation created in Specimen 2 in Soil Type 1 is 42% lower than the deformation of Specimen 1 in the same soil. In Soil Types 2 and 3, this difference is 43% and 11%, respectively. For Specimens 3 and 4, this deformation difference is 25% in Soil Type 1, 25% in Soil Type 2, and 16% in Soil Type 3.

4-4- Effects of Fluid on Deformation

Since the greater thickness of the 10 cm concrete pipe translates into reduced fluid capacity, the fluid has a limited effect on the deformation of this pipe. Therefore, this effect is only discussed for the 5cm-thick concrete pipe.

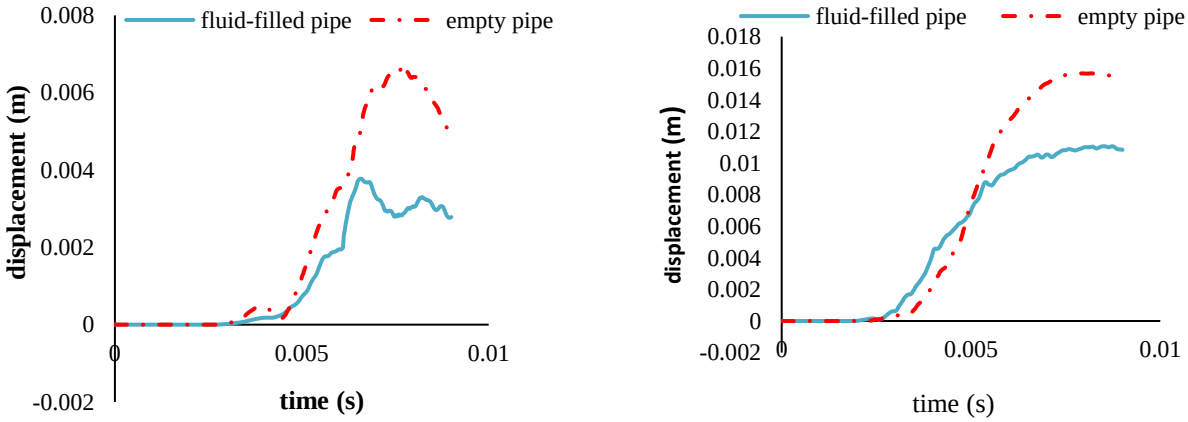

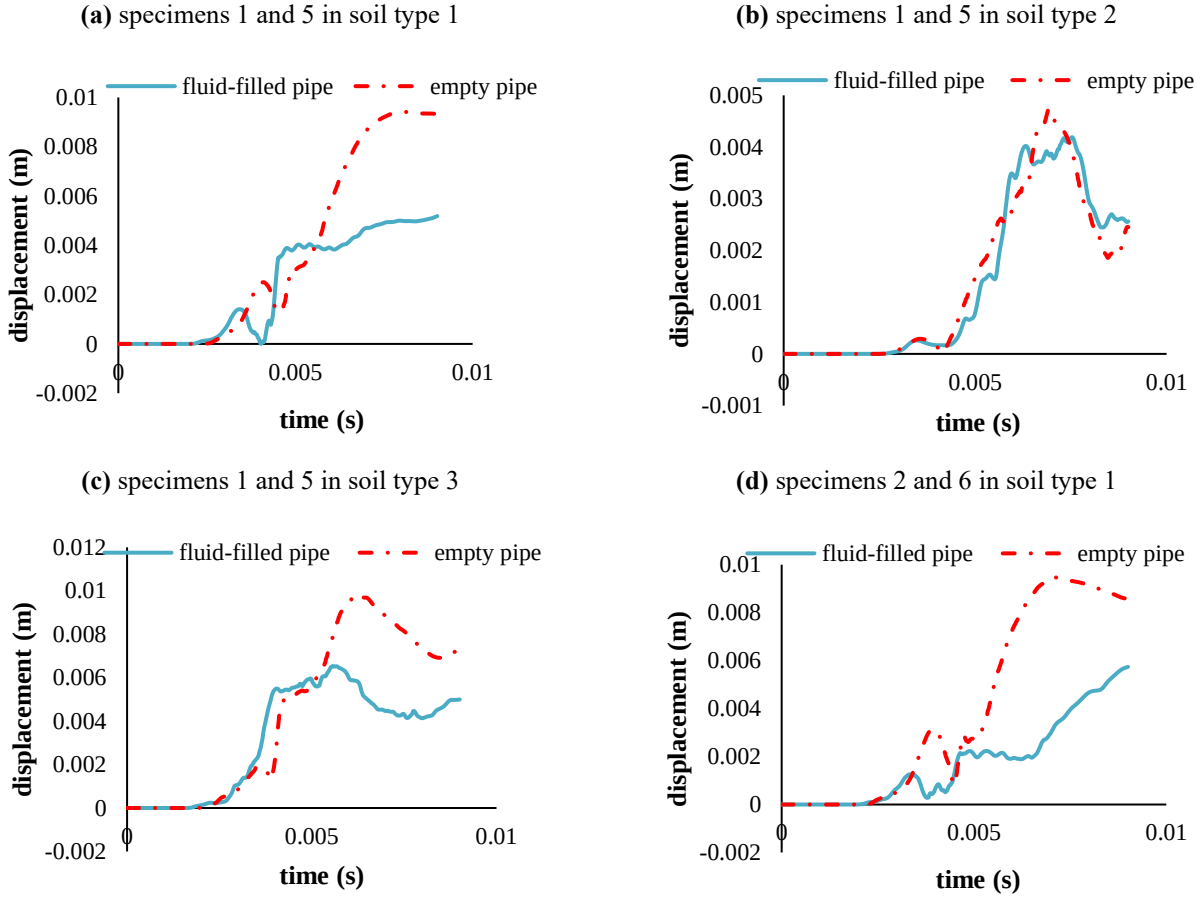

Fig. 9. Comparison of Deformations in Specimens 1, 2, 5, and 6 in Different Soil Types

In Fig. 9, it can be seen that in all soils, the deformation in both types of concrete pipes is less when the pipe is fluid-filled than when it is empty. As noted earlier, this difference can be attributed to the internal pressure caused by the presence of the fluid. From the results presented in Fig.9, it can be concluded that since blast-induced deformation is directed inward, the internal pressure generated because of the presence of the fluid results in reduced deformation in the pipe. For Specimen 1, this reduction is 42% in Soil Type1, 37% in Soil Type 2, and 44% in Soil Type 3. For Specimen 2, these values are 40%, 33%, and 37.3%, respectively. As mentioned earlier, these differences are caused by the internal pressure generated because of the presence of the fluid. Fig. 9 depicts the deformation of concrete pipes with and without fluid.

4.5. Global behavior of empty and fluid-filled concrete pipe type-I in different soils

For concrete pipes, investigations were performed for concrete densities of 2440 and 2500 kg/m^3. The stresses and pressures applied to the empty and fluid-filled concrete pipes in six types of soil are presented in the following tables and

diagrams.

Table 9. The difference pressures applied to empty and fluid-filled concrete pipes in different soils

soil	Concrete pipe 1		
Soil type	pressure applied tofluid-filled pipe (Mpa)	pressure applied to empty pipe (Mpa)	Different (%)
Type 1	35	36	%۲٫۱
Type 2	98	121	%۱۹
Type 3	125	161	%۲۲٫۳

Listed in Table 9 are the differences between the pressures applied to the empty and fluid-filled type-I concrete pipe in six types of soil. This table shows that compared to the pressure on the fluid-filled concrete pipe, the pressure applied to the empty pipe is 2.1% higher in the soil type-1, 19% higher in the soil type-2, 23.3% higher in the soil type-3. As previously mentioned, this difference is due to the lack of internal pressure in the empty pipe.

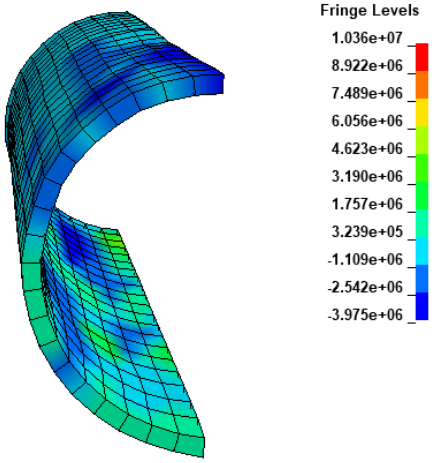

Fig.10. Pressure (pa) applied to the fluid-filled type-I concrete pipe in the soil type-3

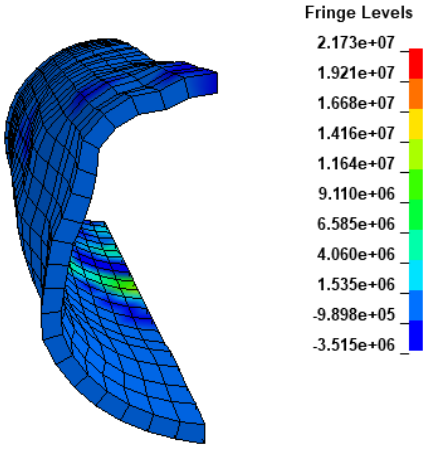

Fig.11. Pressure (pa) applied to the type-I empty concrete pipe in the soil type-3

Fig 10 and 11 indicate that the highest pressure is applied to the top section of pipe at the point directly below the blast source. Figures 12 to 14 portray the pressure applied on the empty and fluid-filled concrete pipes in six types of soil. The results are presented as pressure-time graphs for empty and fluid-filled pipes for a period of 9 milliseconds.

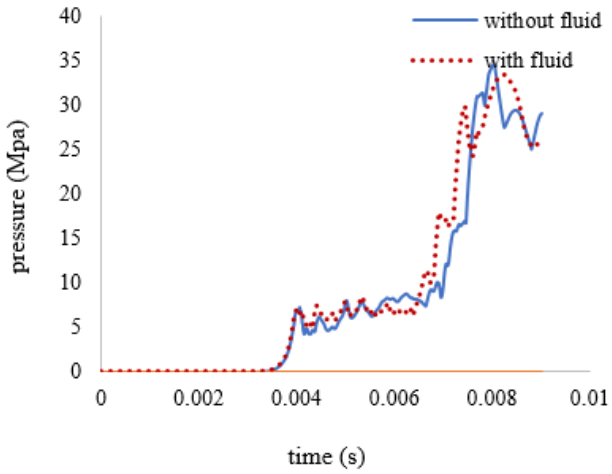

Fig.12. Pressure-time curves of the empty and – fluid type-I concrete pipes in the soil type-1 (for 9 milliseconds)

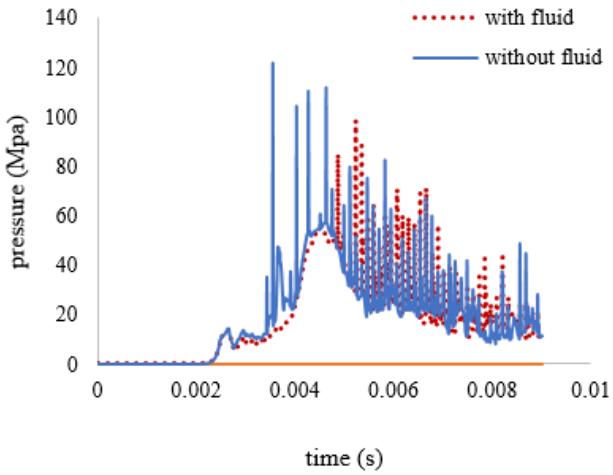

Fig.13. Pressure-time curves of the empty and – fluid type-I concrete pipes in the soil type-2 (for 9 milliseconds)

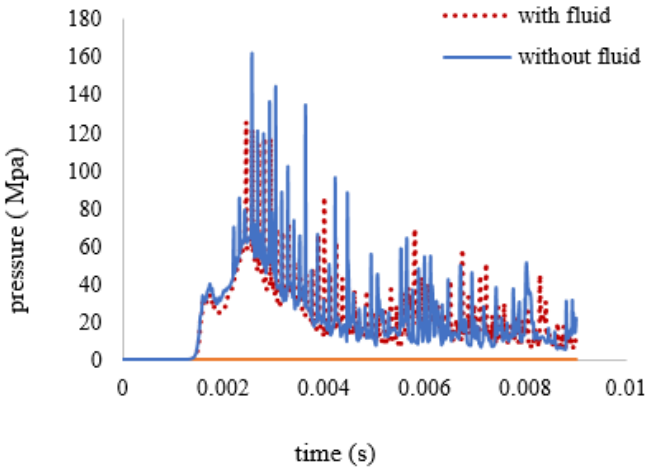

Fig.14. Pressure-time curves of the empty and – fluid type-I concrete pipes in the soil type-3 (for 9 milliseconds)

4-6- Effects of Soil on Pressure and Stress Applied to Concrete and Steel Pipes

In this study, the steel pipes were considered to have a yield strength of 360 MPa. The results obtained by applying the stresses and pressures on the steel and concrete pipes with a thickness of 10 cm in two different soil types with different densities are presented in the Tables 10 and 11.

Table 10. Global Maximum Pressure Applied to Steel and Concrete Pipes in Different Soils

Pressure (Mpa)	Soil 1	Soil 2	Reduction percentage
Concrete pipe type 1 with 10 cm thickness	59	67	12%
steel pipe with 10 cm thickness	243	310	22%

The global pressures obtained for Type I concrete and steel pipes in different soils are compared in Table 10. As can be seen, there is a 12% difference between the pressures obtained for the same concrete pipe in Soil Types 1 and 2. Moreover, the global pressures obtained for steel pipes have a 22% difference in Soil Types 1 and 2. The peak pressure applied to the concrete pipe was 67MPa, which occurred in Soil Type 2. The lowest pressure applied to this pipe was 59MPa, which was observed in Soil Type 1, as can be seen in Table 10. The peak pressure applied to the steel pipe was 310MPa, which occurred in Soil Type 2. The lowest pressure applied to this pipe was 243MPa, which was observed in Soil Type 1. In addition, the effects of soil type on the pressure applied to the pipe are illustrated in Table 10.

Table 11. Global Maximum Stress Applied to Steel and Concrete Pipes in Different Soils

Stress (Mpa)	Soil 1	Soil 2	Reduction percentage
Concrete pipe type 1 with 10 cm thickness	53	57	8%
steel pipe with 10 cm thickness	324	393	21%

As shown in Table 11, increasing the soil density by 24% increased the stress applied to Type I concrete pipe by 8%. For the steel pipe, increasing the soil density by 24% increased the applied stress by 21%. These results highlight the important role of soil density in soil performance during the explosion.

5- Conclusions

This study analysed the behaviour of concrete and steel pipes made of two types of concrete and one type of steel with thicknesses of 5 and 10 cm under the blast load of 6.5 kg TNT in three different soil types over a period of 9 milliseconds. The effects of the presence of a fluid inside the pipe on the blast load-induced strain and deformation and the soil's effects were also studied. The results of this study can be summarized as follows:

In the investigation of the behaviour of concrete pipes in different soils, it was found that the concrete pipe with a higher P-crush behaves better under blast-induced pressure.

Given the amount of plastic strain generated in Specimen 1, this type of pipe fails in both inner and outer surfaces in all three soil types, which means it cannot be used in any of these soils.

If placed in Soil Types 1 or 2, Specimen 2 undergoes failure in both inner and outer surfaces (for 6.5kg TNT), which renders the pipe useless. However, if it is placed in Soil Type 3, the pipe will remain usable.

In all soil types, the amount of strain generated on the outer surface of Specimen 3 exceeds the permissible plastic strain limit, which indicates that there will be a

failure on the pipe's surface. However, the strain created on the inner surface of the pipe is less than the permissible limit, indicating that it will remain internally intact under the blast load.

Comparison of the amounts of strain generated in Specimen 4 in Soil Types 1 and 3 with the permissible limit shows that both the internal and external surfaces of this pipe remain intact under the blast load. In Soil Type 2, the outer surface sustains damage, but the internal surface remains intact, keeping the pipe usable.

The depth of damage in different areas of Specimens 3 and 4 ranges from 2 cm to 7 cm. In the analysis of the effects of the fluid on the deformation in Specimens 1 and 2, it is found that the presence of the fluid in the pipe creates an internal pressure, increasing the resistance against the blast force induced pressure applied from the soil, thereby reducing the overall deformation of the pipe. Density plays an immensely important role in the magnitude of stress to be transferred from the soil to the pipeline. For Specimen 1, this reduction is 42% in Soil Type 1, 37% in Soil Type 2, and 44% in Soil Type 3. For Specimen 2, these values are 40%, 33%, and 37.3%, respectively. The plastic strain generated in Specimen 1 in Soil Type 1 is 85% higher than the allowed plastic strain of the concrete pipe. This value is 87% for Soil Type 2 and 85% for Soil Type 3.

6- References

[1]. Kouretzis, G. P., Bouckovalas, G. D., & Gantes, C. J. (2007). Analytical calculation of blast-induced strains to buried pipelines. International Journal of Impact Engineering, 34(10), 1683-1704. https://doi.org/10.1016/j.ijimpeng.2006.08.008.

[2]. Francini, R. B., & Baltz, W. N. (2008). Blasting and construction vibrations near existing pipelines: what are appropriate levels. In 2008 7th International Pipeline Conference (pp. 519-531). American Society of Mechanical Engineers Digital Collection. https://doi.org/10.1115/IPC2008-64325

[3]. Riedel W, Mayrhofer C, Thoma K, et al. (2010) Engineering and numerical tools for explosion protection of engineering and numerical tools for explosion protection of reinforced concrete. International Journal of Protective Structures 1(1): 85–102.

[4]. Nourzadeh, D., Khorshid, S., Takada, S., & Bargi, K. (2011). Analytical proposal to damage assessment of buried continuous pipelines during external blast loading. Eng Tech, 5, 11-20.

[5]. Yan, S., Xu, Y. R., & Chang, H. Y. (2012). Numerical simulation of dynamic response of buried pipeline by ground explosion. In Earth and Space 2012: Engineering, Science, Construction, and Operations in Challenging Environments (pp. 1159-1166).

[6]. Xu, G. F., Deng, Z. D., Deng, F. F., & Liu, G. B. (2013). Numerical simulation on the dynamic response of buried pipelines subjected to blast loads. In Advanced Materials Research (Vol. 671, pp. 519-522). Trans Tech Publications.

[7]. Jing, X. F., Cai, Z. Y., & Liu, K. H. (2014). Numerical Simulation of Response of Explosion Ground Shock to Buried Gas Pipeline. In Applied Mechanics and Materials (Vol. 448, pp. 3970-3974). Trans Tech Publications.

[8]. Orton, S. L., Chiarito, V. P., Minor, J. K., & Coleman, T. G. (2013). Analysis of CFRP Strengthened Reinforced Concrete Structural Components Subjected to Close-in Blasts. International Journal of Protective Structures, 4(4), 467-483.

[9]. Mokhtari, M., & Nia, A. A. (2015). A parametric study on the mechanical performance of buried X65 steel pipelines under subsurface

detonation. Archives of Civil and Mechanical Engineering, 15(3), 668-679.

[10]. Alamatian, E., & Zahabi, H. (2015). Analysis of the Effect of Explosion on Altering the Tensions and Strains in Buried Water Pipes. Journal of Engineering Science & Technology Review, 8(3).

[11]. Abedi, A. S., Hataf, N., & Ghahramani, A. (2016). Analytical solution of the dynamic response of buried pipelines under blast wave. International Journal of Rock Mechanics and Mining Sciences, 88,301-306. https://doi.org/10.1016/j.ijrmms.2016.07.014

[12]. Mokhtari, M., & Nia, A. A. (2016). The application of CFRP to strengthen buried steel pipelines against subsurface explosion. Soil Dynamics and Earthquake Engineering, 87, 52-62. https://doi.org/10.1016/j.soildyn.2016.04.009

[13]. Zhang, L., Liang, Z., & Zhang, J. (2016). Mechanical response of a buried pipeline to explosion loading. Journal of Failure Analysis and Prevention, 16(4), 576-582. https://doi.org/10.1007/s11668-016-0121-2

[14]. Parviz, M., Aminnejad, B., & Fiouz, A. (2017). Numerical simulation of dynamic response of water in buried pipeline under explosion. KSCE Journal of Civil Engineering, 21(7), 2798-2806. https://doi.org/10.1007/s12205-017-0889-y

[15]. Vivek, P., & Sitharam, T. G. (2017). The effect of spherical air blast on buried pipelines: a laboratory simulation study. International Journal of Physical Modelling in Geotechnics, 18(2), 57-67. https://doi.org/10.1680/jphmg.16.00070.

[16]. Adibi, O., Azadi, A., Farhanieh, B., & Afshin, H. (2017). A parametric study on the effects of surface explosions on buried high pressure gas pipelines. Engineering Solid Mechanics, 5(4), 225-244. DOI: 10.5267/j.esm.2017.9.003

[17]. Guo, Y., Liu, C., Wang, D., & He, R. (2018). Numerical study and safety spacing of buried parallel gas pipelines: a study based on TNT equivalent method. International Journal of Pressure Vessels and Piping, 168, 246-257. https://doi.org/10.1016/j.ijpvp.2018.11.002

[18]. Kakaei, R., & Hajiazizi, M. (2021). The effect of GFRP on reinforcing the buried and internally pressurized steel pipes against terrorist attacks. International Journal of Pressure Vessels and Piping, 189, 104273. https://doi.org/10.1016/j.ijpvp.2020.104273

[19] Holmquist, T.J., G.R. Johnson, and W.H. Cook. A Computational Constitutive Model for Concrete Subjected to Large Strains, High Strain Rates and High Pressures. in 14th International symposium, Vol2; Warhead mechanisms, terminal ballistics. 1993. Arlington: ADPA.

[20] Mata, G.A., Evaluation of Concrete Constitutive Models for Impact Simulations, in Mechanical Engineering ETDs. 2017, THE UNIVERSITY OF NEW MEXICO.

[21]. Chen, Y. F., & Yi, G. X. (2013). Dynamic response analysis of the reinforced concrete column under the effect of explosive impact load. In Advanced Materials Research (Vol. 681, pp. 99-104). Trans Tech Publications. https://doi.org/10.4028/www.scientific.net/AMR.681.99

[22]. Chen, X., Xu, L., & Zhu, Q. (2017). Mechanical behavior and damage evolution for concrete subjected to multiple impact loading. KSCE Journal of Civil Engineering, 21(6), 2351-2359. https://doi.org/10.1007/s12205-016-1143-8

[23]. Krieg, R. D. (1972). A simple constitutive description for cellular concrete. Albuquerque, NM: Sandia National Laboratories.

[24]. Busch, C. L., & Tarefder, R. A. (2017). Evaluation of appropriate material models in LS-DYNA for MM-ALE finite element simulations of small-scale explosive airblast tests on clay soils. Indian Geotechnical Journal, 47(2), 173-186.